Ultrasonics 56 (2015) 545–550

Contents lists available at ScienceDirect

Ultrasonics

journal homepage: www.elsevier.com/locate/ultras

# Reversible influence of ultrasound on $\gamma$-irradiated Mo/*n*-Si Schottky barrier structure

O.Ya. Olikh *

*Faculty of Physics, Taras Shevchenko Kyiv National University, Kyiv 01601, Ukraine*

ARTICLE INFO

*Article history:*
Received 17 February 2014
Received in revised form 17 September 2014
Accepted 5 October 2014
Available online 13 October 2014

*Keywords:*
Dynamic ultrasonic influence
Schottky barrier
Gamma-ray effect
Silicon

ABSTRACT

The influence of ultrasonic loading on current–voltage characteristics has been investigated in Mo/*n*-$n^+$-Si structures irradiated by $^{60}$Co $\gamma$-rays. The longitudinal ultrasonic waves were of 9.6 MHz in frequency and had the intensity approaching 1.3 W/cm$^2$. The observed reversible acoustically induced increase in forward and reverse currents was as large as 60%. The ultrasound has been found to affect thermionic emission mainly due to Schottky barrier height decrease. The observed effects are related to acoustically induced ionization of the defects located at the metal–semiconductor interface. It has also been found that in the result of $\gamma$-irradiation, the ultrasonic wave-defect interaction is modified. Ultrasonic loading, however, has been found to have no effect either on direct or phonon-assisted tunneling.



## 1. Introduction

The structures with Schottky contacts are known to be widely applied in high-speed logic circuits, integrated and optoelectronic technologies. The electrical characteristics of such structures depend on various defects. Therefore any alteration of a defect system results in modified Schottky diode characteristics. For example, the variations of Schottky barrier height (SBH), ideality factor and reverse current were observed after $\gamma$-irradiation of metal–semiconductor structures [1–6]. Moreover, the values of these characteristics often change non-monotonically depending on the absorbed dose [3–6]. On the other hand, in recent years, ultrasonic (US) waves were found to affect various properties of semiconductors. In particular, US treatment causes the modification of silicon surface state spectrum [7], the increase of metal cluster size in silicon oxide [8,9], the change of paramagnetic properties of silicon nanoclusters in $SiO_2$ [10], as well as the modification of different optical properties of semiconductor structures [11–14]. Moreover, under the action of US waves the electrical properties of barrier structure reveal both residual [15–17] and reversible (dynamic) [18,19] changes. In addition, by applying US treatment, the radiation defects (RDs) in semiconductors can be annealed [20–23]. Unfortunately, nearly all the reports dealing with acoustically stimulated effects in irradiated structures are mainly concerned with applying high ultrasound power and residual modification of properties, while the works that focus on the reversible acoustically induced effects are very few.

Our goal is to investigate experimentally the dynamic variations of electrical characteristic which take place in $\gamma$-irradiated Mo/*n*-$n^+$-Si structures in the result of US loading. The investigation would provide not only better understanding of US wave – defect interaction but could also facilitate the development of acoustically controlled devices or radiation sensors.

## 2. Experimental details

The samples used in our experiments were 0.2 μm thick *n*-Si:P epitaxial layer on 250 μm thick $n^+$-Si:Sb substrate. The diameter of molybdenum Schottky contact fabricated on the epi-layer surface was 2 mm.

The investigated structures were exposed to $^{60}$Co $\gamma$-ray radiation. The cumulative dose $D_\gamma$ was 0 kGy, 10 kGy and 100 kGy for samples M0, M10 and M100 respectively.

The substrate carrier concentration was $4.2 \cdot 10^{22}$ m$^{-3}$. The epi-layer carrier concentration $N_d$ was monitored by measuring capacity–voltage ($C$–$V$) characteristics: the slope $d(1/C^2)/dV$ of the plotted curve obtained for dependence $1/C^2$–$V$ showed [24] that $N_d$ was $1.15 \cdot 10^{23}$ m$^{-3}$, $1.10 \cdot 10^{23}$ m$^{-3}$ and $1.19 \cdot 10^{23}$ m$^{-3}$ for M0, M10, and M100 respectively.

The current–voltage ($I$–$V$) characteristics of the samples both with and without US loading were measured at room temperature. In case of US loading, the longitudinal waves excited in the samples were 9.6 MHz in frequency and had the intensity of $W_{US} < 1.3$ W/cm$^2$.

* Corresponding author.
*E-mail address:* olikh@univ.kiev.ua

http://dx.doi.org/10.1016/j.ultras.2014.10.008
0041-624X/

In order to avoid the effect of piezoelectric field on *I–V* characteristics, the piezoelectric cell was shielded — see Fig. 1. The sample temperature was controlled by differential copper-constantan thermocouple. Since the sample heated due to US loading, this was taken into account in the calculations of acoustically induced changes of the parameters. To identify the charge-transport mechanisms in the structures under study, the *I–V* characteristics were measured in the temperature range from 260 to 330 K without US loading.

## 3. Results and discussion

Fig. 2 shows the *I–V* characteristics that were measured for Mo/*n*-Si structures both with and without US loading. It can be seen that the forward current as well as the reverse current increases under the action of ultrasound. The increase in the values depends on both bias voltage and the degree of $\gamma$-irradiation. It should be emphasized that all the acoustically induced variations of the structure parameters (Figs. 2, 6, 9 and 10) are reversible, i.e., they relax after US loading (the falling time was approximately ten minutes). In order to better understand the possible causes of US influence, we have analyzed the charge transport mechanisms in the samples under study.

### 3.1. Forward current

Suppose the thermionic emission (TE) is the dominant charge transport mechanism, then the Schottky diode forward current $I_F$ can be expressed as in [25,26]:

$$I = I_S \exp\left(\frac{q(U_F - I_F R_S)}{nkT}\right)\left[1 - \exp\left(-\frac{q(U_F - I_F R_S)}{kT}\right)\right], \quad (1)$$

where $I_S = AA^*T^2 \exp(-\Phi_B/kT)$ is the saturation current, $A$ is the diode area, $A^*$ is the effective Richardson constant of 112 A cm$^{-2}$ K$^{-2}$ for *n*-Si [24], $\Phi_B$ is zero bias SBH, $n$ is the ideality factor, $U_F$ is the forward bias, $R_S$ is the series resistance. To evaluate $R_S$ from *I–V* characteristics, we used Gromov's method [26] and then plotted the dependence of $\ln(I_F/\{1 - \exp[-q(U_F - I_F R_S)/(kT)]\})$ on $U_F$. The plot slope and intercept provide $n$ and $I_S$ (and $\Phi_B$) respectively.

According to [25], in case of TE current flowing through homogeneous metal–semiconductor contact (i) SBH is expected to decrease with temperature increase in the way similar to semiconductor band gap $E_G$; (ii) the temperature dependence of $n$ can be described as follows

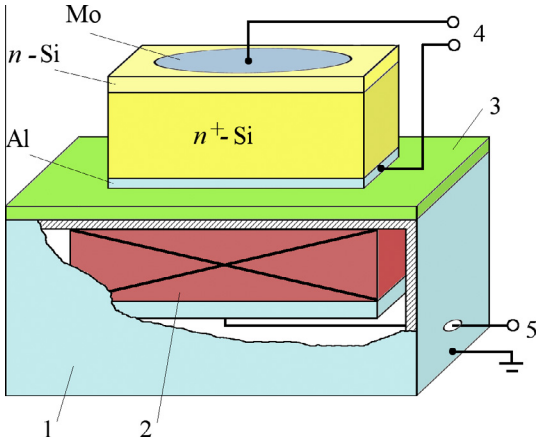


**Fig. 1.** Schematic of the ultrasonic loading. 1 — Electric shield; 2 — piezoelectric transducer; 3 — dielectric layer (mica); 4 and 5 — contact to *I–V* measure and to ultrasound excitate respectively.

$$n = 1 + T_0/T, \quad (2)$$

where $T_0$ is a constant over a wide temperature range.

Figs. 3 and 4 present the obtained temperature dependences of $\Phi_B$ and $n$ as well as the temperature dependence of $E_G$ calculated by using the Varshni equation $E_G = 1.169 - 7.021 \cdot 10^{-4}\, T^2/(T + 1108)$ [27].

The dependences predicted by the TE theory of homogeneous contact have been observed experimentally only for M100. On the other hand, the behavior of the experimentally obtained dependences for M0 and M10 can be related to SBH inhomogeneity (patches) available in the samples [28,29]. According to the model of inhomogeneous contact with patchwork regions

$$\Phi_B = \Phi_B^0 - q\sigma_\Phi^2/2kT, \quad (3)$$

$$(n^{-1} - 1) = \rho_2 - q\rho_3/2kT, \quad (4)$$

where $\Phi_B^0$ is the SBH of the region outside the patches, $\sigma_\Phi$ deals with the distribution of patch parameters, $\rho_2$ and $\rho_3$ are the coefficients that quantify the bias deformation of SBH distribution. As seen in Fig. 5, the dependences of $\Phi_B$ and $(n^{-1} - 1)$ on the inverse temperature are linear for M0 and M10.

In our opinion, the modification of charge transport mechanism is connected with the gettering of negative point RDs by the patches. At low irradiation level (10 kGy), the accumulation of RDs depends on patch parameters; as a result the parameter distribution becomes broader: $\sigma_\Phi = 100$ mV for M10 is greater than $\sigma_\Phi = 40$ mV for non-irradiated sample M0. After the structures were $\gamma$-irradiated with $D_\gamma = 100$ kGy, all the patches became completely shielded and did not affect the forward current.

As seen from Fig. 6, US loading leads to the SBH decrease whereas the ideality factor remains almost unchanged (except for M10). In our experiments the SBH decreased by $(13 \pm 4)$ mV at $W_{US} \simeq 0.7$ W/cm$^2$ and did not vary until $W_{US} \simeq 0.4$ W/cm$^2$. It follows from (3) that $\Phi_B$ variation can be due to modification of both $\Phi_B^0$ and $\sigma_\Phi$. However, it is shown in [30] that $\sigma_\Phi$ deals with $n$ ($n = 1 + q\sigma_\Phi^2/(3kTV_{bb})$, where $V_{bb} = \Phi_B - (kT/q)\ln(N_c/N_d) - U$, $N_c$ is the effective density of states in the conduction band). But the acoustically induced variation of ideality factor has not been found for M0 (Fig. 6(b)), therefore it is $\Phi_B^0$ that varies under US loading. In our opinion, the reversible SBH decrease is caused by the acoustically induced ionization of interface defects. It should be noted that the acoustically induced defect ionization was also reported in [31,32]. In turn, the ionization takes place due to the oscillation of misfit dislocations. As for the threshold behavior of the $\Phi_B$, the significant decrease at $W_{US} \simeq 0.4$ W/cm$^2$ is associated with a considerable increase of oscillation peak in conditions of US loading if the dislocations are released from stoppers.

It has been found, that

(i) The US influence efficiency fells off after $\gamma$-irradiation: the SBH decrease does not exceed 10 mV for M100 and 3 mV for M10 at $W_{US} > 1$ W/cm$^2$.
(ii) The dependence SBH on $W_{US}$ has no threshold for the irradiated samples.
(iii) For irradiated samples the increase in $D_\gamma$ leads to the increase of SBH variation under US loading.

In our opinion, the US effect mechanism transforms due to irradiation: the RD gettering results in dislocation pinning, and linear defects are no more able to interact effectively with US waves although the value of $W_{US}$ is the same as before $\gamma$-irradiation. On the other hand, point RDs (e.g., divacancies or A-centers) are able to interact with ultrasound [23]. As a result, if the SBH decrease for M10 and M100 is due to acoustic ionization of point RDs, then acoustically induced effect should to enhance with the increase in

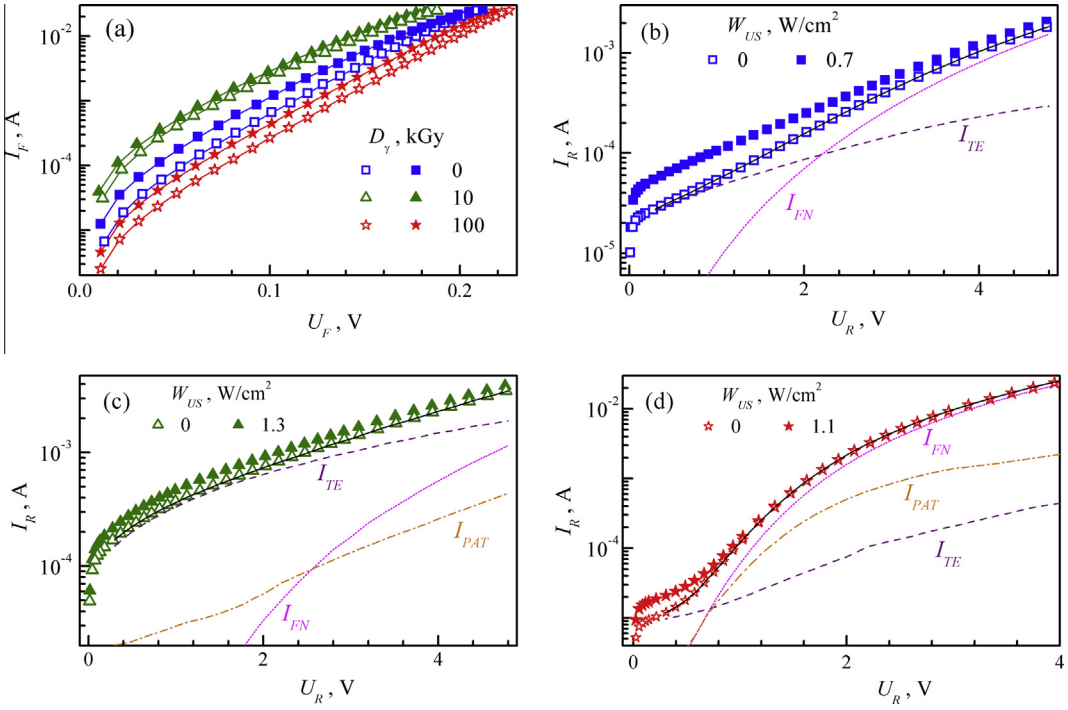


**Fig. 2.** Forward (a) and reverse (b–d) *I–V* characteristics of Mo/*n*-Si Schottky structures at $T = 305$ K. Filled and empty marks are the experimental results measured with and without US loading respectively. Solid lines are calculated by using (1) and (5). Dotted lines represent a different component of the reverse current. $D_\gamma$, kGy: 0 (a and b), 10 (a and c), 100 (a and d).

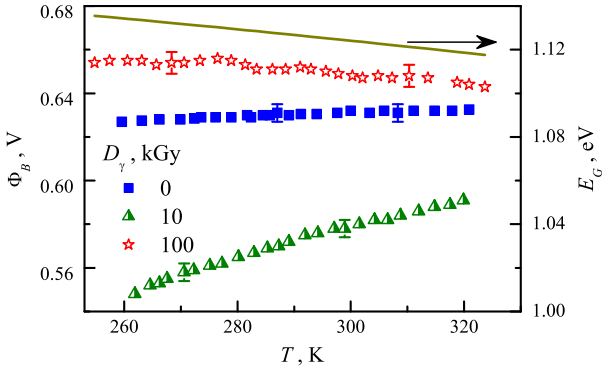


**Fig. 3.** Temperature dependences of zero bias SBH. The line is the temperature dependence of silicon band gap.

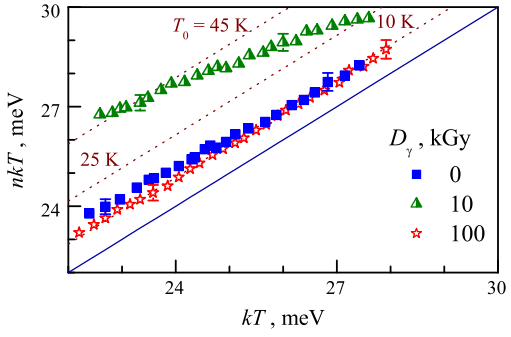


**Fig. 4.** Temperature dependences of the current inverse slope. Dashed lines are calculated by using (2) with different T0 value. The solid line is ideal case $n = 1$.

$D_\gamma$ and RD concentration, which has been observed in our experiments (Fig. 6). We also believe that ultrasound affects patch shielding in the irradiated samples, and this is the reason why the acoustically induced variation of ideality factor is observed only for the sample exposed to a medium dose (M10).

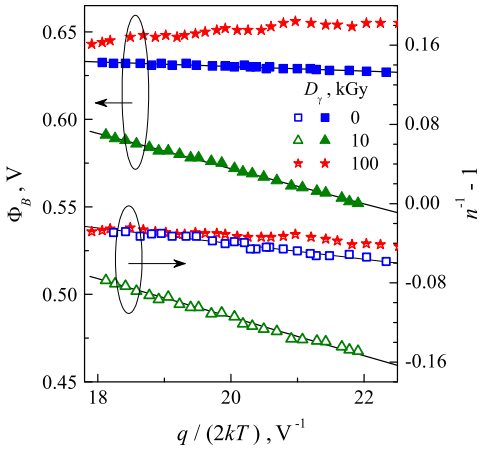


**Fig. 5.** Zero bias SBH and $(n^{-1} - 1)$ versus $q/(2kT)$. Marks are the experimental results, lines are the least-squares linear fitting.

### 3.2. Reverse current

The experimental dependence of reverse current $I_R$ can be described as follows

$$I_R(T, U_R) = C_{TE}(U_R)T^2 \exp[-E_{TE}(U_R)/kT] + I_{FN}(U_R) + I_{PAT}(T, U_R) \quad (5)$$

That is, the current in the structures under study is caused by three different mechanisms. The bias dependences of the components at room temperature are shown in Fig. 2(b)–(d).

The component $I_{TE} = C_{TE}T^2 \exp(-E_{TE}/kT)$ describes TE current. The characteristic energy $E_{TE}$ deals with SBH [25] and depends on

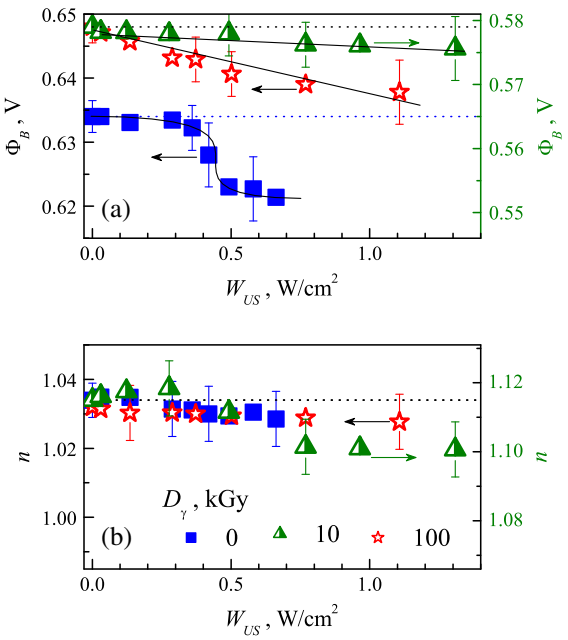


**Fig. 6.** Dependences of the SBH (a) and the ideality factor (b) on the US intensity for samples with the different $D_\gamma$. Horizontal dashed lines represent the parameter values measured without US loading.

the bias. In our experiments the dependence $E_{TE} \sim V_{bb}^{2/3}$ was observed for M0, which is typical for inhomogeneous contact [28].

The dependences of component $I_{FN}$ on $F$ ($F = (2qN_dV_{bb}/\varepsilon_0\varepsilon)^{1/2}$ is the electric field at metal–semiconductor interface, $\varepsilon = 11.7$ is Si dielectric constant) are plotted in Fig. 7 in Fowler–Nordheim coordinates. The linearity of the field dependences and independence of $I_{FN}$ on temperature are indicative of the tunneling mechanism of $I_{FN}$ component.

In case of tunneling across triangular barrier, the modified Fowler–Nordheim equation can be used [25,33]:

$$\ln(I_{FN}/F^2) \propto -4\sqrt{2m^*}(qE_{D,eff})^{3/2}/(3\hbar qF) \tag{6}$$

where $m^*$ is the electron effective mass (for Si, $m^* = 1.08 \cdot 9.11 \cdot 10^{-31}$ kg), $E_{D,eff}$ is the effective tunneling energy. If the model of tunneling through the deep center is valid, then the energy depth of the center $E_D$ deals with $E_{D,eff}$ as follows [34]:

$$E_{D,eff} = E_G\left\{\frac{3}{16}\left[\frac{\pi}{2} - \arcsin\left(1-\frac{2E_D}{E_G}\right)\right] - \frac{3}{8}\left(1-\frac{2E_D}{E_G}\right)\sqrt{\frac{E_D}{E_G}-\left(\frac{E_D}{E_G}\right)^2}\right\}^{2/3} \tag{7}$$

The value of $E_D = (120 \pm 5)$ mV was obtained by using (7) and linear fitting of the data in Fig. 7 for each of the samples. The obtained value is close to the acceptor level of interstitial carbon $C_I$ $E_C - (0.10–0.12)$ eV [35,36]. In addition, $C_I$ is the secondary RD in $\gamma$-irradiated silicon [35]. In our case, the value of $I_{FN}$ increases after irradiation, especially for M100 (Fig. 7). Therefore, $I_{FN}$ component can be associated with the direct tunneling through the deep levels of $C_I^-$.

The component $I_{PAT}$, which is observed in the irradiated structures only, grows as $D_\gamma$ is increased. The origin of the new charge transport mechanism after $\gamma$-irradiation is a reported phenomenon; according to [2,3], for example, the reasons for additional current may be generation–recombination process or tunneling.

It is known [34,37] that phonon-assisted tunneling involving deep centers can be a reason of the current arising in metal–semiconductor structures. According to [34,37] the emission rate $P$ increases exponentially with $F$ : $P(F,T) = P(0,T)\exp(F^2/F_0^2)$, where $F_0$ is characteristic field strength, given by

$$F_0^{-2/3} \propto \sqrt[3]{\frac{q^2\hbar^2}{24k^3m^*}}\,\frac{1}{T}. \tag{8}$$

The dependence $\ln I_{PAT} \sim F^2$ has been observed for the structures under study. The slope of dependence $F_0^{-2/3} = [d(\ln I_{PAT})/d(F^2)]^{1/3}$ depends linearly on the inverse temperature (see Fig. 8). The values obtained by linear fitting of the data in Fig. 8 ($2.9 \cdot 10^{-3}$ and $0.6 \cdot 10^{-3}$ K m$^{2/3}$ V$^{-2/3}$ for M10 and for M100 respectively) are comparable to the theoretical value $q^2\hbar^2/(24k^3m^*) = 1.7 \cdot 10^{-3}$ K m$^{2/3}$ V$^{-2/3}$. Thus, the reverse current $I_{PAT}$ is caused by the phonon-assisted tunneling involving RD deep centers.

In order to estimate the influence of ultrasound we used the relative reverse current variation $\varepsilon I_{US} = (I_{R,US} - I_{R,0})/I_{R,0}$, where $I_{R,US}$ and $I_{R,0}$ are the reverse currents in the samples at the same temperature, with and without US loading respectively.

Fig. 9 shows that the reverse current increases by tens of per cents under US loading and the efficiency of US radiation influence fells off as the reverse bias $U_R$ increases. The contribution of TE component decreased with the bias increase as well — see Fig. 2(b)–(d). In fact, if $I_{TE}$ is dominant, then the acoustically induced variation of reverse current is observed. Hence, ultrasound affects only thermionic emission and does not affect both direct and phonon-assisted tunneling. In particular, this indicates that the center with ionization energy 0.12 eV ($C_I$) does not take part in US wave – defect interaction.

Furthermore, it should be stressed that if $I_{TE}$ is dominant ($U_R < 0.7$ V for M100), then $I_R$ (Fig. 10) vary in the same way as SBH does (Fig. 6 (a)). Actually, it can be seen that (i) the US loading effect decreases after irradiation; (ii) the threshold on the

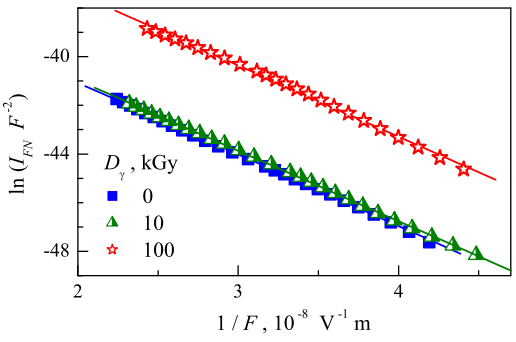


**Fig. 7.** Fowler–Nordheim plots of the temperature-independent component of the reverse current. Marks represent the experimental data, lines are the least-squares linear fitting.

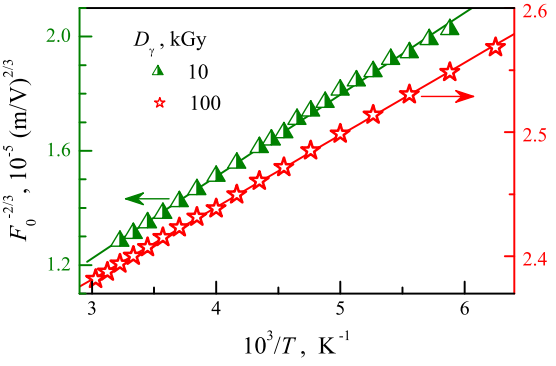


**Fig. 8.** The slope of the field dependence of the reverse current component $I_{PAT}$ versus inverse temperature.Marks represent the experimental data, lines are the least-squares linear fitting.

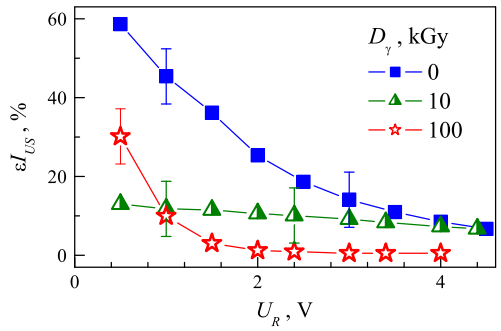


**Fig. 9.** Dependences of acoustically induced variations in the reverse current on bias. $W_{US}$, W/cm$^2$: 0.6 (M0), 1.3 (M10), 1.1 (M100). $T$ = 305 K.

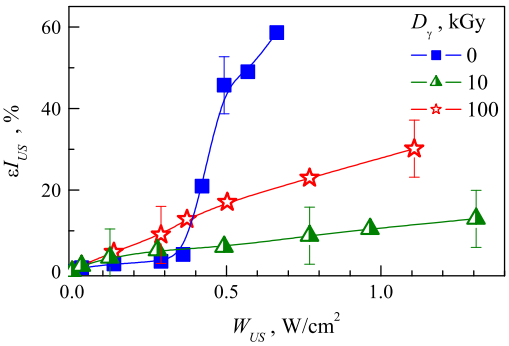


**Fig. 10.** Dependences of relative reverse current variations on ultrasonic intensity. $U_R$ = 0.5 V. $T$ = 305 K.

dependence of US effect on $W_{US}$ disappears after irradiation; (iii) the acoustically induced variation of irradiated sample reverse current enhances with $D_\gamma$ increase. Thus, the influence of ultrasound on the reverse current is related to the interaction between the US wave and dislocations (for non-irradiated structures) or point RDs (for irradiated structures) in the way that has been described above.

## 4. Conclusion

The experimental investigation of ultrasound influence on the electric properties of Mo/$n$-$n^+$-Si Schottky barrier structure has revealed that both forward and reverse current of the Schottky barrier structure increases under the action of ultrasonic radiation; $\gamma$-irradiation of the structure results in qualitative modification of ultrasound effect. The ultrasonic waves have been shown to affect thermionic emission due to decrease in Schottky barrier height. The analysis has shown that the observed effects can be accounted for by the ionization of interface defects due to ultrasonic wave – dislocation interactions in non-irradiated structures and ultrasound – point defect interactions in irradiated structures. It has been found that ultrasonic loading has practically no effect on both direct and phonon-assisted tunneling and, moreover, the center with the ionization energy of 0.12 eV is acoustically non-active. Thus, ultrasound can be an effective tool for controlling metal–semiconductor structure characteristics.

## References


[1] A. Tataroglu, S. Antindal, Gamma-ray irradiation effects on the interface states of MIS structures, Sens. Actuat., A 151 (2) (2009) 168–172, http://dx.doi.org/10.1016/j.sna.2009.02.035.

[2] O. Gullu, M. Cankaya, M. Biber, A. Turut, Gamma irradiation-induced changes at the electrical characteristics of organic-based Schottky structures, J. Phys. D: Appl. Phys. 41 (13) (2008) 135103, http://dx.doi.org/10.1088/0022-3727/41/13/135103.

[3] S. Karatas, A. Turut, S. Altindal, Effects of $^{60}$Co $\gamma$-ray irradiation on the electrical characteristics of Au/n-GaAs (MS) structures, Nucl. Instrum. Methods Phys. Res., Sect. A 555 (1–2) (2005) 260–265, http://dx.doi.org/10.1016/j.nima.2005.09.017.

[4] S. Karatas, A. Turut, Electrical properties of Sn/p-Si (MS) Schottky barrier diodes to be exposed to $^{60}$Co $\gamma$-ray source, Nucl. Instrum. Methods Phys. Res., Sect. A 566 (2) (2006) 584–589, http://dx.doi.org/10.1016/j.nima.2006.07.054.

[5] A. Tataroglu, S. Antindal, Analysis of interface states and series resistance at MIS structure irradiated under $^{60}$Co $\gamma$-rays, Nucl. Instrum. Methods Phys. Res., Sect. A 580 (3) (2007) 1588–1593, http://dx.doi.org/10.1016/j.nima.2007.07.027.

[6] O.Y. Olikh, Non-monotonic $\gamma$-ray influence on Mo/n-Si Schottky barrier structure properties, IEEE Trans. Nucl. Sci. 60 (1) (2013) 394–401, http://dx.doi.org/10.1109/TNS.2012.2234137.

[7] N. Zaveryukhina, E. Zaveryukhina, S. Vlasov, B. Zaveryukhin, Acoustostimulated changes in the density of surface states and their energy spectrum in p-type silicon single crystals, Tech. Phys. Lett. 34 (3) (2008) 241–243, http://dx.doi.org/10.1134/S106378500803019X.

[8] A. Romanyuk, V. Spassov, V. Melnik, Influence of in situ ultrasound treatment during ion implantation on formation of silver nanoparticles in silica, J. Appl. Phys. 99 (3) (2006) 034314, http://dx.doi.org/10.1063/1.2171773.

[9] A. Romanyuk, P. Oelhafen, R. Kurps, V. Melnik, Use of ultrasound for metal cluster engineering in ion implanted silicon oxide, Appl. Phys. Lett. 90 (1) (2007) 013118, http://dx.doi.org/10.1063/1.2430055.

[10] M. Jivanescu, A. Romanyuk, A. Stesmans, Influence of in situ applied ultrasound during Si+ implantation in $SiO_2$ on paramagnetic defect ginflapplied, J. Appl. Phys. 107 (11) (2010) 114307, http://dx.doi.org/10.1063/1.3369041.

[11] A. Romanyuk, V. Melnik, Y. Olikh, J. Biskupek, U. Kaiser, M. Feneberg, K. Thonke, P. Oelhafen, Light emission from nanocrystalline silicon clusters embedded in silicon dioxide: role of the suboxide states, J. Lumin. 130 (1) (2010) 87–91, http://dx.doi.org/10.1016/j.jlumin.2009.07.021.

[12] A. El-Bahar, S. Stolyarova, A. Chack, R. Weil, R. Beserman, Y. Nemirovsky, Ultrasound treatment for porous silicon photoluminescence enhancement, Phys. Stat. Solidi A 197 (2) (2003) 340–344, http://dx.doi.org/10.1002/pssa.200306521.

[13] E. Zobov, M. Zobov, F. Gabibov, I. Kamilov, F. Manyakhin, E. Naimi, Effect of ultrasonic treatment on photoelectric and luminescent properties of ZnSe crystals, Semiconductors 42 (3) (2008) 277–280, http://dx.doi.org/10.1134/S1063782608030068.

[14] I. Ostrovskii, O. Korotchenkov, O. Olikh, A. Podolyan, R. Chupryna, M. Torres-Cisneros, Acoustically driven optical phenomena in bulk and low-dimensional semiconductors, J. Opt. A: Pure Appl. Opt. 3 (4) (2001) S82–S86, http://dx.doi.org/10.1088/1464-4258/3/4/364.

[15] V. Melnik, Y. Olikh, V. Popov, B. Romanyuk, Y. Goltvyanskii, A. Evtukh, Characteristics of silicon pn junction formed by ion implantation with in situ ultrasound treatment, Mater. Sci. Eng., B 124–125 (2005) 327–330, http://dx.doi.org/10.1016/j.mseb.2005.08.039.

[16] O. Olikh, T. Pinchuk, Acoustic wave corrected current–voltage characteristics of GaAs-based structures with Schottky contacts, Tech. Phys. Lett. 32 (6) (2006) 517–519, http://dx.doi.org/10.1134/S1063785006060204.

[17] A. Davletova, S.Z. Karazhanov, A study of electrical properties of dislocation engineered Si processed by ultrasound, J. Phys. Chem. Solids 70 (6) (2009) 989–992, http://dx.doi.org/10.1016/j.jpcs.2009.05.009.

[18] A. Sukach, V. Teterkin, Ultrasonic treatment-induced modification of the electrical properties of InAs p–n junctions, Tech. Phys. Lett. 35 (6) (2009) 514–517, http://dx.doi.org/10.1134/S1063785009060108.

[19] O. Olikh, Effect of ultrasonic loading on current in Mo/n-n+-Si with Schottky barriers, Semiconductors 47 (7) (2013) 987–992, http://dx.doi.org/10.1134/S106378261307018X.

[20] N. Guseynov, Y. Olikh, S. Askerov, Ultrasonic treatment restores the photoelectric parameters of silicon solar cells degraded under the action of $^{60}$Co gamma radiation, Tech. Phys. Lett. 33 (1) (2007) 18–21, http://dx.doi.org/10.1134/S1063785007010063.

[21] P. Parchinskii, S. Vlasov, L. Ligai, Effect of ultrasonic treatment on the generation characteristics of irradiated silicon–silicon-dioxide interface, Semiconductors 40 (7) (2006) 808–811, http://dx.doi.org/10.1134/S106378260607013X.

[22] A. Gorb, O. Korotchenkov, O. Olikh, A. Podolian, Ultrasonically recovered performance of $\gamma$-irradiated metal–silicon structures, IEEE Trans. Nucl. Sci. 57 (3) (2010) 1632–1639, http://dx.doi.org/10.1109/TNS.2010.2047655.

[23] Y. Olikh, M. Tymochko, A. Dolgolenko, Acoustic-wave-stimulated transformations of radiation defects in $\gamma$-irradiated n-type silicon crystals, Tech. Phys. Lett. 32 (7) (2006) 586–589, http://dx.doi.org/10.1134/S106378500607011X.

[24] D.K. Schroder, Semiconductor Material and Device Characterization, 3rd Edition., John Wiley & Sons, New Jersey, 2006.

[25] E.H. Rhoderick, R.H. Williams, Metal Semiconductor Contacts, second ed., Clarendon Press, Oxford, 1988.

[26] D. Gromov, V. Pugachevich, Modified methods for the calculation of real schottky-diode parameters, Appl. Phys. A 59 (3) (1994) 331–333, http://dx.doi.org/10.1007/BF00348239.

[27] J. Munguia, J.-M. Bluet, O. Marty, G. Bremond, M. Mermoux, D. Rouchon, Temperature dependence of the indirect bandgap in ultrathin strained silicon on insulator layer, Appl. Phys. Lett. 100 (10) (2012) 102107, http://dx.doi.org/10.1063/1.3691955.

[28] R.T. Tung, Electron transport at metal–semiconductor interfaces: general theory, Phys. Rev. B 45 (23) (1992) 13509–13523, http://dx.doi.org/10.1103/PhysRevB.45.13509.
[29] D. Korucu, A. Turut, H. Efeoglu, Temperature dependent *I–V* characteristics of an Au/n-GaAs Schottky diode analyzed using Tungs model, Phys. B 414 (2013) 35–41, http://dx.doi.org/10.1016/j.physb.2013.01.010.
[30] F. Iucolano, F. Roccaforte, F. Giannazzo, V. Raineri, Temperature behavior of inhomogeneous Pt/GaN Schottky contacts, Appl. Phys. Lett. 90 (9) (2007) 092119, http://dx.doi.org/10.1063/1.2710770.
[31] O. Olikh, Features of dynamic acoustically induced modification of photovoltaic parameters of silicon solar cells, Semiconductors 45 (6) (2011) 798–804, http://dx.doi.org/10.1134/S1063782611060170.
[32] O. Korotchenkov, H. Grimmliss, Long-wavelength acoustic-mode-enhanced electron emission from Se and Te donors in silicon, Phys. Rev. B. 52 (20) (1995) 14598–14606, http://dx.doi.org/10.1103/PhysRevB.52.14598. URL http://link.aps.org/doi/10.1103/PhysRevB.52.14598.
[33] Y.N. Novikov, Non-volatile memory based on silicon nanoclusters, Semiconductors 43 (8) (2009) 1040–1045, http://dx.doi.org/10.1134/S1063782609080144.
[34] S.V. Bulyarskii, A.V. Zhukov, An analysis of the charge-transport mechanisms defining the reverse current–voltage characteristics of the metal-GaAs barriers, Semiconductors 35 (5) (2001) 539–542, http://dx.doi.org/10.1134/1.1371618.
[35] V.S. Vavilov, V.F. Kiselev, B.N. Mukashev, Defects in the Bulk and at the Surface of Silicon, Nauka, Moscow, 1990.
[36] L. Song, B. Benson, G. Watkins, Identification of a bistable defect in silicon: the carbon interstitial-carbon substitutional pair, Appl. Phys. Lett. 51 (15) (1987) 1155–1157, http://dx.doi.org/10.1063/1.98717.
[37] S.D. Ganichev, E. Ziemann, W. Prettl, I.N. Yassievichand, A.A. Istratov, E.R. Weber, Distinction between the Poole–Frenkel and tunneling models of electric-field-stimulated carrier emission from deep levels in semiconductors, Phys. Rev. B 61 (15) (2000) 10361–10365, http://dx.doi.org/10.1103/PhysRevB.61.10361.